

## Playing the tricks of numbers of light sources

Huanyang Chen<sup>1,3</sup>, Yadong Xu<sup>1</sup>, Hui Li<sup>1</sup> and Tomáš Tyc<sup>2</sup>

<sup>1</sup> School of Physical Science and Technology, Soochow University, Suzhou, Jiangsu 215006, People's Republic of China

<sup>2</sup> Faculty of Science and Faculty of Informatics, Masaryk University, Kotlarska 2, 61137 Brno, Czech Republic

E-mail: [chy@suda.edu.cn](mailto:chy@suda.edu.cn)

*New Journal of Physics* **15** (2013) 093034 (14pp)

Received 17 June 2013

Published 23 September 2013

Online at <http://www.njp.org/>

doi:10.1088/1367-2630/15/9/093034

**Abstract.** Transformation optics has demonstrated its ability to design various novel devices, for example, to change objects' sizes, positions or even shapes. This time we come to another magical manipulation: to change the numbers of sources. In this paper, we will design a new class of gradient index lenses from multivalued optical conformal mapping. We shall call them the conformal lenses. Such lenses can make one active source appear omnidirectionally as two (or many) in-phase sources, each interfering with others. As a self-interference phenomenon, this has not been discussed before. Meanwhile, they can transform multiple in-phase sources into one. Other intriguing illusion effects are also demonstrated. Based on the Riemann sheet analysis, the physics mechanism of such effects are well explained. Finally, we apply transmutation methods to design lenses without any singular material parameters.

<sup>3</sup> Author to whom any correspondence should be addressed.



Content from this work may be used under the terms of the [Creative Commons Attribution 3.0 licence](https://creativecommons.org/licenses/by/3.0/). Any further distribution of this work must maintain attribution to the author(s) and the title of the work, journal citation and DOI.

**Contents**

<b>1. Introduction</b>	<b>2</b>
<b>2. Mapping of <math>w^2 = z^2 - 1</math></b>	<b>2</b>
<b>3. ‘1 to 2’ and ‘2 to 1’</b>	<b>3</b>
<b>4. Other illusion effects</b>	<b>4</b>
<b>5. Riemann sheet analysis</b>	<b>6</b>
<b>6. Transmutation of the singularities</b>	<b>9</b>
<b>7. General mapping <math>w^N = z^N - 1</math></b>	<b>11</b>
<b>8. Conclusions</b>	<b>12</b>
<b>Acknowledgments</b>	<b>13</b>
<b>References</b>	<b>13</b>

**1. Introduction**

Gradient index lenses [1], such as the Maxwell fish-eye lens [2], the Luneburg lens [3] and the Eaton lens [4] have recently drawn much attention because of their utility for designing invisibility cloaks [5], omnidirectional retroreflectors [6] and various imaging functionalities [7–12] including the perfect imaging [13–15]. Transformation optics [5, 16], as a newly versatile tool, have also succeeded in designing various novel devices [17, 18], including invisibility cloaks [19–26]. Generally, materials designed by transformation optics are inhomogeneous and anisotropic. In particular, such anisotropic materials are often of magnetic response, leading to challenges in implementation. Optical conformal mapping [5] however, can be applied to obtain isotropic and non-magnetic response materials, thereby facilitating the implementation. There have been some optical conformal devices proposed, such as a beam collimator [27–29] and beam bend [30]. In this paper, we will design a new class of gradient index lenses based on a simple optical conformal mapping. Such lenses can transform one active source into two and two into one. They can also create other illusion effects, such as obtaining a rotated image for one current sheet like the field rotator does [31], or transforming a ‘+’ sign into a ‘-’ sign and vice versa. By analyzing the Riemann sheet, we found the intrinsic physics mechanism of the illusion effects. In addition, we can even remove the singular values of the material parameters using the transmutation methods [32, 33]. Finally, we suggest a group of multivalued conformal mappings to design lenses that can transform one source into many, and vice versa. Note that the functionality of transforming two sources into one has been proposed based on the overlapped illusion optics [34], yet requiring negative index materials.

**2. Mapping of  $w^2 = z^2 - 1$** 

We will start the story from the conformal mapping

$$w^2 = z^2 - 1, \quad (1)$$

which maps  $w$ -space ( $w = u + iv$ ) into  $z$ -space ( $z = x + iy$ , two values of  $w$  are mapped into two values of  $z$ ).

From the theory of optical conformal mapping [5], we should have the relationship of the refractive indexes in  $w$ -space ( $n_w$ ) and  $z$ -space ( $n_z$ ),

$$n_z = n_w \left| \frac{dw}{dz} \right|, \quad (2)$$

by keeping the optical path unchanged during the mapping. In this case, if we suppose  $n_w = 1$  (vacuum in  $w$ -space), the refractive index in  $z$ -space should be

$$n_z = \frac{|z|}{\sqrt{|z^2 - 1|}} = \sqrt{\frac{x^2 + y^2}{\sqrt{(x^2 - y^2 - 1)^2 + 4x^2y^2}}}. \quad (3)$$

Writing in bipolar coordinates, we have

$$n_z = \sqrt{\frac{\cosh \tau + \cos \sigma}{2}}, \quad (4)$$

where  $x = \frac{\sinh \tau}{\cosh \tau - \cos \sigma}$  and  $y = \frac{\sin \sigma}{\cosh \tau - \cos \sigma}$ . We will find that it is hopeful to write in this form in the later sections, e.g. section 6. From equations (3) and (4), it is clear that three singular points can be found, i.e. when  $z = 0$ ,  $n_z = 0$ , when  $z = \pm 1$ ,  $n_z = +\infty$ . There are two kinds of special mappings here. One is that  $z = 0$  is mapped to  $w = \pm i$  (one point mapped to two points). The other is that  $z = \pm 1$  are mapped to  $w = 0$  (two points mapped to one point). These two properties would be used to demonstrate the following important functionalities, i.e. transforming one source into two, and two into one. The transformation media described in equations (3) and (4) are called the conformal lenses, which can work for active sources in both the wave optics realm and the geometric optics limit.

It is important to note that optical conformal mapping usually requires materials to be filled in the whole space. However, for the mapping in equation (1), when  $z \rightarrow \infty$ ,  $w \rightarrow z$ , we can introduce a cut-off radius  $r_c$  so that

$$n_z = \begin{cases} 1, & |z| > r_c, \\ \frac{|z|}{\sqrt{|z^2 - 1|}}, & |z| \leq r_c, \end{cases} \quad (5)$$

indicating that the lens here is of finite size, with almost the same properties reserved as the full one in equations (3) and (4) if  $r_c$  is large enough. We will use this finite-size lens to demonstrate the intriguing wave functionality by performing the numerical simulations below.

### 3. '1 to 2' and '2 to 1'

We will only consider the transverse electric polarized waves (i.e.  $\varepsilon_z = n_z^2$ ,  $\mu = 1$ ) and the line current sources. For the transverse magnetic polarized waves, if we choose  $\mu_z = n_z^2$  and  $\varepsilon = 1$ , the effects will be the same. Here we assign  $r_c = 5$  and the wavelength  $\lambda = 2$  (arbitrary units). Figure 1(a) shows the electric field distribution when there is one current source (with a '1 A' current) located at the position  $z = 0$  in the conformal lens described by equation (5). The far field distribution (in the region  $r \geq r_c$ ) appears to be that of two line current sources (each with a '1/2 A' current) located at  $w = \pm i$  in vacuum, which is illustrated in figure 1(b). In other words, one source is transformed into two. Figure 1(c) shows the electric field distribution when there are two line current sources located at the positions  $z = \pm 1$  in the lens. Each one carries '1 A' current. The far field distribution appears to be that of only one line current source with a '2 A' current in vacuum, which is illustrated in figure 1(d). In other words, two sources are transformed into one.

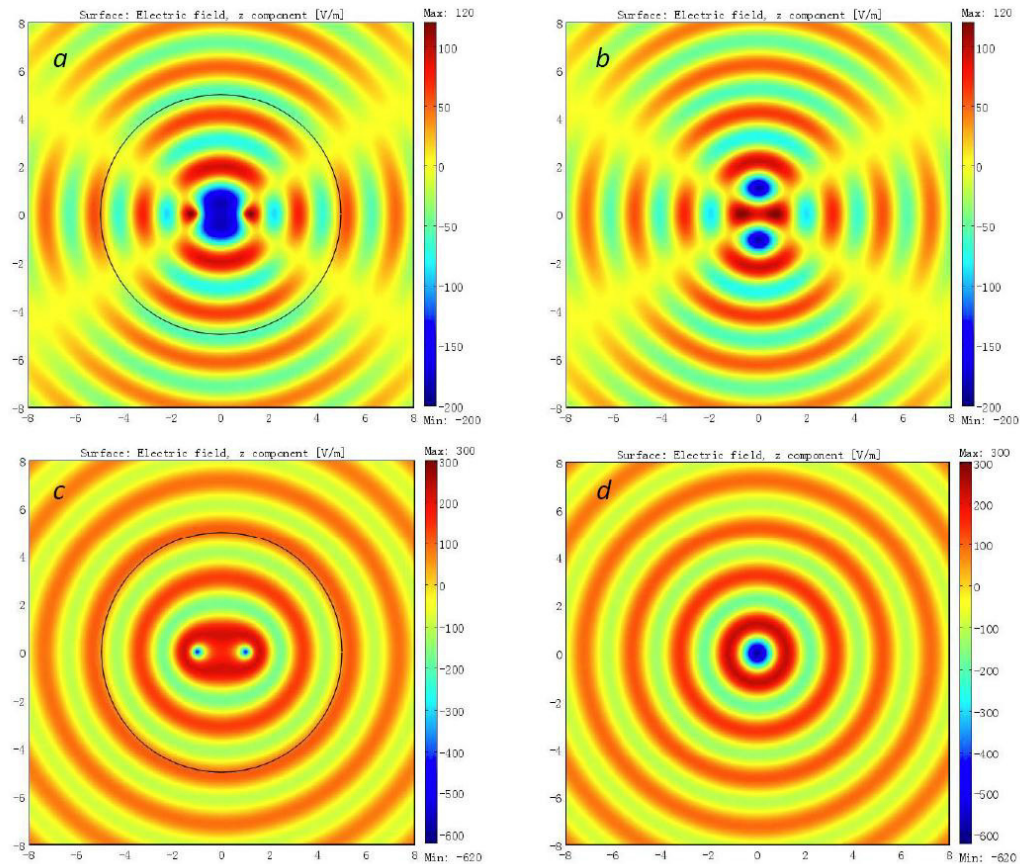


**Figure 1.** The electric field distribution for (a), one line current source with a ‘1 A’ current in the conformal lens described by equation (5); (b), two line current sources (each with a ‘1/2 A’ current) in vacuum; (c), two line current sources (each with a ‘1 A’ current) in the lens; (d), one line current source with a ‘2 A’ current in vacuum.

#### 4. Other illusion effects

In this section, we will introduce five additionally intriguing properties of the conformal lenses for other active sources, such as current sheets. In the previous section, we mainly focused on point-to-point mappings, while here we will work on line-to-line mappings.

First of all, let us consider the two mappings below. One is that one line (from  $z = -i$  to  $i$ ) is mapped into two lines (from  $w = -\sqrt{2}i$  to  $i$  and from  $w = i$  to  $\sqrt{2}i$ ). The other is that two lines (from  $z = -\sqrt{2}$  to  $-1$  and from  $z = 1$  to  $\sqrt{2}$ ) are mapped into one line (from  $w = -1$  to  $1$ ). Again, numerical simulations will be used in describing such properties. We assign  $r_c = 5$ , the wavelength  $\lambda = 2$  and  $E_z = 1 \text{ V m}^{-1}$  for each line boundary (the same applies in the following). The resembling far-field patterns in figures 2(a) and (b) show that one current sheet appears to be two, while those in figures 2(c) and (d) tell us that two current sheets are transformed into one.

Next, we will consider another mapping, where a line (from  $z = -1$  to  $1$ ) is mapped into another (from  $w = -i$  to  $i$ ). Figures 3(a) and (b) show almost identical far field distributions, indicating that one current sheet has a  $90^\circ$  rotation image when embedded in the conformal lens.

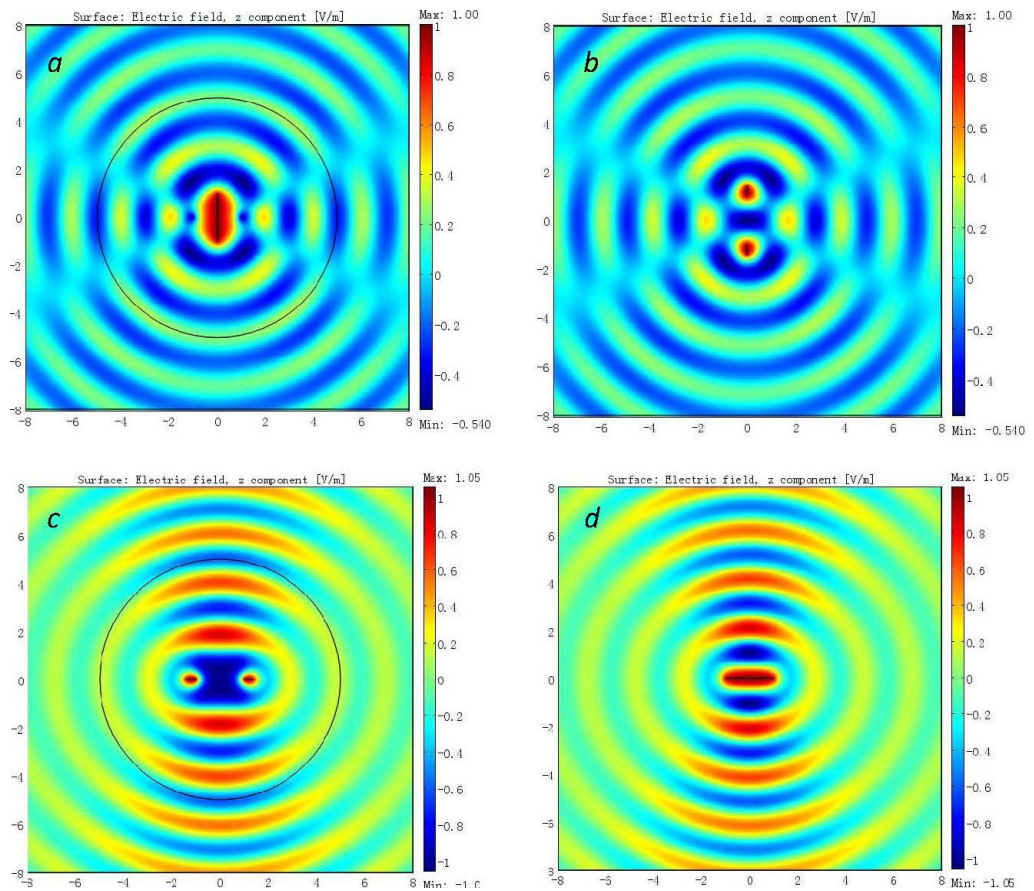


**Figure 2.** The electric field distribution for (a) one current sheet in the conformal lens; (b) two current sheets in vacuum; (c) two current sheets in the lens; (d) one current sheet in vacuum.

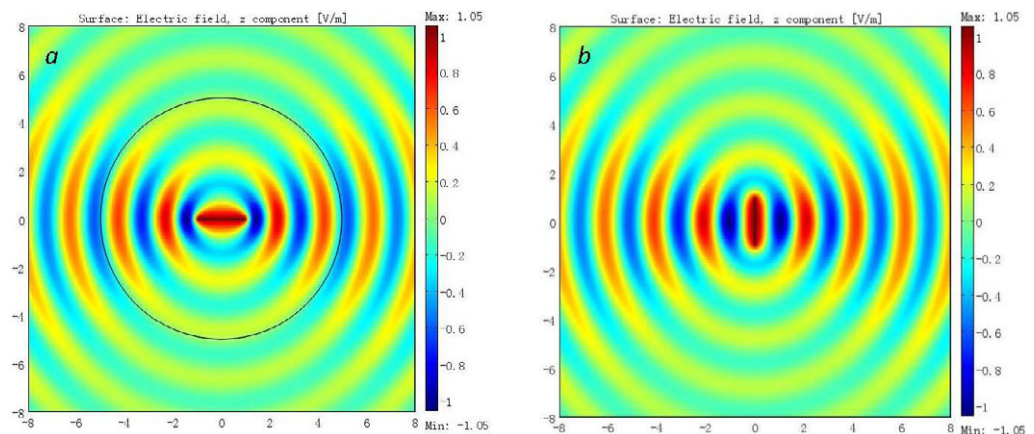


**Figure 3.** The electric field distribution for (a) one current sheet in the conformal lens; (b) a rotated current sheet in vacuum.

Thirdly, let us come to another two interesting mappings. One is that two cross lines (one is from  $z = -1$  to  $1$ , while the other is from  $z = -i$  to  $i$ ) are mapped into one single line (from  $w = -\sqrt{2}i$  to  $\sqrt{2}i$ ). The other mapping is that a line (from  $z = -\sqrt{2}$  to  $\sqrt{2}$ ) is mapped into

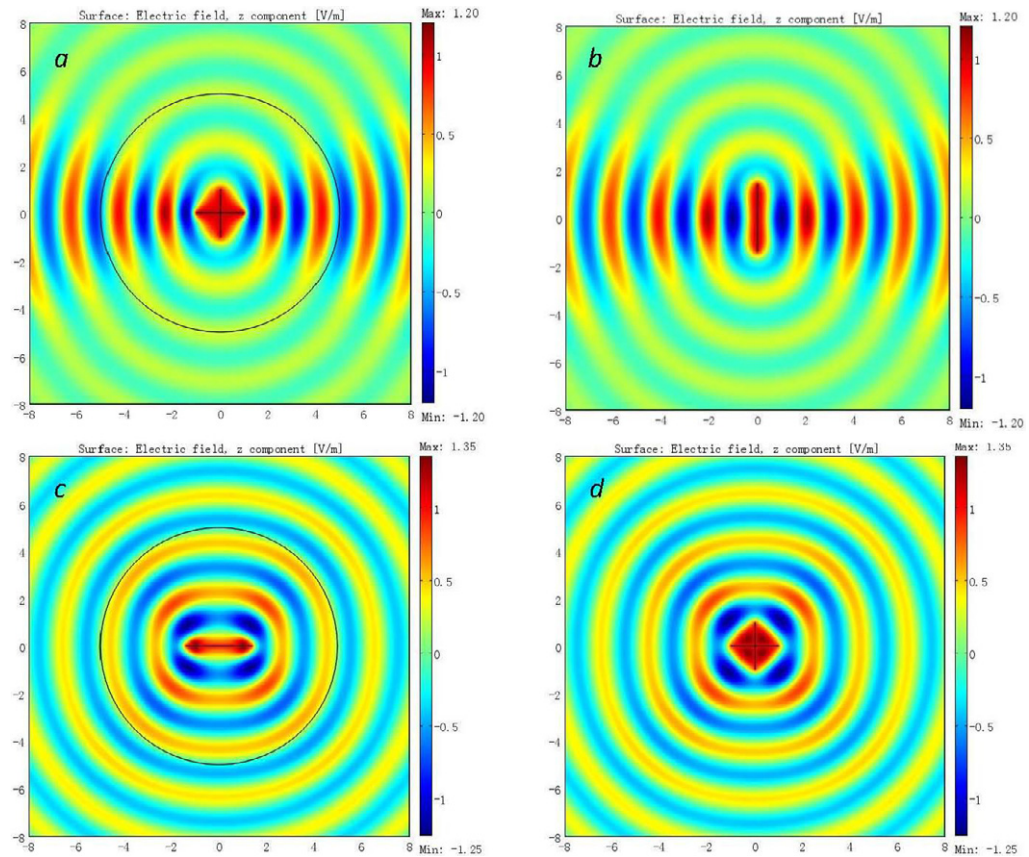


**Figure 4.** The electric field distribution for (a) two cross current sheets in the conformal lens; (b) one current sheet in vacuum; (c) one current sheet in the lens; (d) two cross current sheets in vacuum.

two cross lines (one is from  $w = -1$  to  $1$ , while the other is from  $w = -i$  to  $i$ ). Figures 4(a) and (b) show that the conformal lens can transform two cross current sheets into one current sheet (i.e. a ‘+’ sign into a ‘-’ sign). Figures 4(c) and (d) show that a ‘-’ sign appears to be a ‘+’ sign if it is embedded in the lens. These illusion effects can be treated as combinations of the above rotation effects and the effects of transforming one source into two and two into one. For example, the combination of figures 2(a) and 3(a) becomes figure 4(a).

## 5. Riemann sheet analysis

As we have seen, the mapping  $w^2 = z^2 - 1$  can effectively transform one source into two and vice versa. To understand the mechanism beyond this in more detail, it is useful to look closer at light propagation from a single point source in both electromagnetic and real spaces. Suppose that the source is located at the point  $z_0$  of physical space with  $\text{Re}(z_0) > 0$ . In virtual space this point corresponds to the point  $w_0 = \sqrt{z_0^2 - 1}$ , where the branch of the square root is chosen such that  $\text{Re}(w_0) > 0$ . In terms of geometrical optics, the point source illuminates both Riemann sheets of virtual space: the upper sheet is illuminated directly with the exception of the shadow cast by the branch cut, and the lower sheet is illuminated by the rays that enter it from the upper

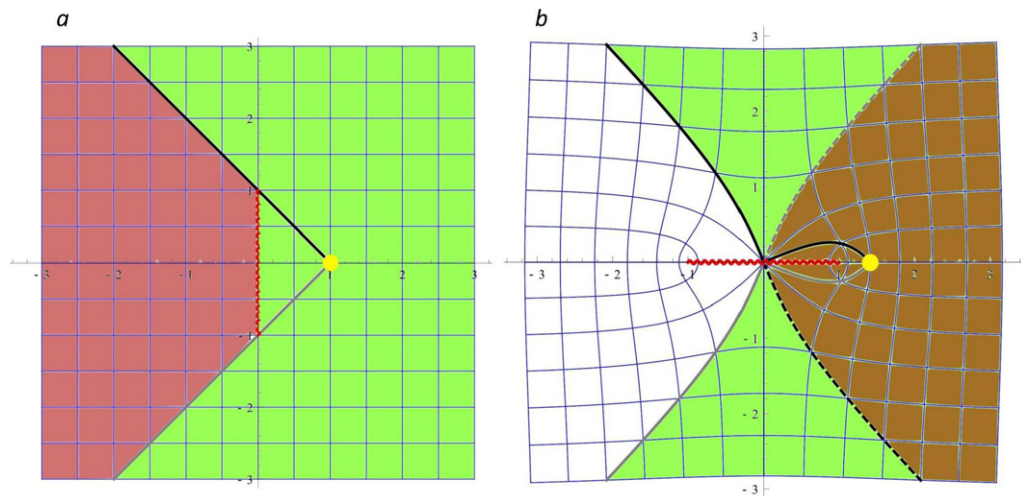


**Figure 5.** Regions illuminated by a point source in virtual space ( $u-v$  space) and physical space ( $x-y$  space). The source (yellow) is placed at  $w = 1$  of virtual space, which corresponds to  $z = \sqrt{2}$  of physical space. The branch cuts are shown by the red zigzag lines. (a) In virtual space, the source illuminates a part of the upper Riemann sheet directly (shown in green), and a part of the lower Riemann sheet via the branch cut (pink region). The borders of these regions are marked by the thick black and gray lines. (b) In physical space, the two corresponding regions partly overlap, which causes interference in the green-pink region. The white region cannot be accessed by any ray from the source, so it remains dark. The images of the thick (black and gray) lines on upper and lower Riemann sheets of virtual space are shown by full and dashed style, respectively.

sheet via the branch cut, see figure 5(a). Since both Riemann sheets of virtual space are mapped to the same physical space, the images of their illuminated regions may overlap in general. This indeed happens, as figure 5(b) reveals, and points of the green-pink region can be accessed from the source by two different rays. In that region therefore interference fringes occur, see figure 6(a). At the same time, some points in physical space can be reached from the source by a single ray only (those in the green region in our example of figure 5(b)), and still others cannot be reached by any ray (white region). If there is another source at  $z = -z_0$  with the same phase, all the regions can be accessed from the sources by two different rays. Therefore the interference fringes occur everywhere, see figure 6(b) where we set  $z_0 = \sqrt{2}$ . The field pattern looks like that when there are two sources at  $w = \pm 1$  with the same phase in vacuum, as plot in figure 6(c) for comparison.

Suppose now that the source is placed on the branch cut in physical space. Its image in virtual space lies on the branch cut as well, i.e. on the imaginary axis between  $i$  and  $-i$ . Then, apparently, both Riemann sheets are illuminated entirely, so the overlap region in physical space is the whole  $z$ -plane. This way, interference fringes are observed in the whole plane, and asymptotically they look the same as if they were created by a pair of sources in vacuum,

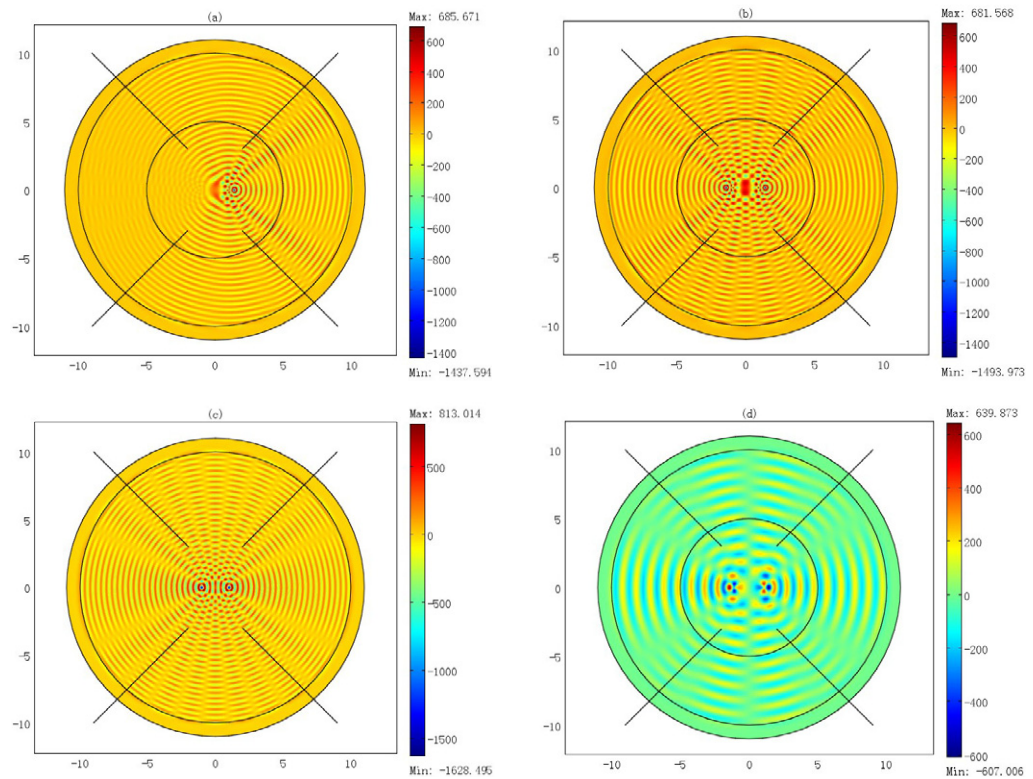


**Figure 6.** (a) Wave from a single source as in figure 5(b) with the vacuum wavelength  $\lambda = 0.4$ . The approximate boundary of the overlap region is shown by the two black lines on the right, the approximate boundary of the shadow region is shown by the two black lines on the left. Interference fringes in the overlap region are clearly visible. (b) Wave from two sources at  $z = \pm\sqrt{2}$  with the same phase and  $\lambda = 0.4$ . (c) Wave from two sources at  $w = \pm 1$  with the same phase in vacuum for comparison. (d) Wave from two sources at  $z = \pm\sqrt{2}$ , differing in phase by  $\pi$ , with  $\lambda = 1$ .

just as we have seen in figure 1(a) in section 3. Figure 7(a) shows the interference pattern for the single source at  $z = 0$  for the wavelength  $\lambda = 0.4$ .

Now consider a different situation. If the source in physical space is located at  $z = 1$ , the overlap region will be the whole half-plane  $\text{Re}(z) > 0$  while the shadow region will be the whole half-plane  $\text{Re}(z) < 0$ ; the roles of these half-planes will be reversed if the source is at  $z = -1$  instead. Moreover, at both of these source positions the virtual space source position is the origin, so the interference in the overlap region is always perfectly constructive. Further, when there are both the sources at  $z = \pm 1$ , each of them radiates mainly into its corresponding half-plane. If they are in phase, the wave in the half-plane  $\text{Re}(z) > 0$  goes smoothly to the wave in the half-plane  $\text{Re}(z) < 0$ , so the total field is smooth as we have seen in figure 1(c) in section 3. However, if the phase of the two sources differs by  $\pi$ , then there will be a phase jump along the imaginary axis, which will result in destructive interference there, as can be seen in figure 7(b). Similar phenomenon occurs when the two sources with a  $\pi$  phase difference are located at  $z = \pm\sqrt{2}$ , see figure 6(d). In detail, the green regions in figure 5(b) have similar field patterns as



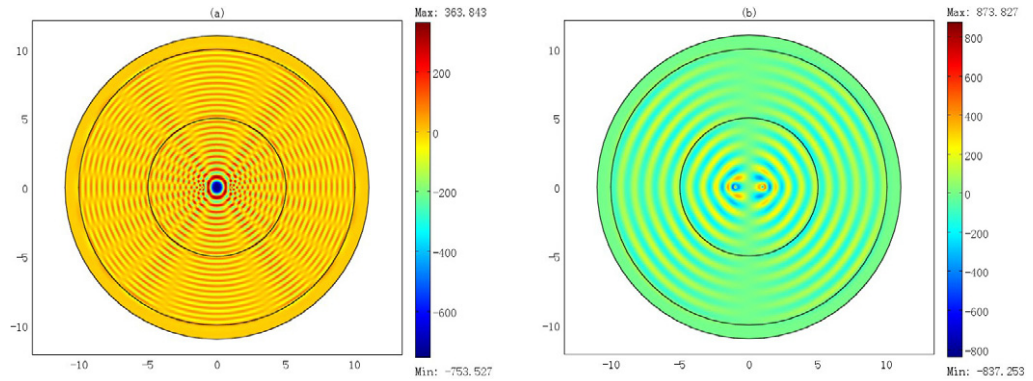


**Figure 7.** Wave pattern for (a), a single source in physical space placed at  $z = 0$  with  $\lambda = 0.4$ , and (b), two sources placed at  $z = \pm 1$ , differing in phase by  $\pi$ , with  $\lambda = 1$ .

those from two sources with a  $\pi$  phase difference at  $w = \pm 1$  in vacuum, while the white region and the green-pink region have similar field patterns as those from two sources with the same phase at  $w = \pm 1$  in vacuum. More complicated combinations of sources can be arranged to have various illusion effects. However, careful analysis of different interference regions should be made following the above scheme.

This way, it is the unusual properties of the two-to-two mapping  $w^2 = z^2 - 1$  that cause one source to look like two and vice versa. As we will see, the situation can be extended to higher powers of  $w$  and  $z$  as well.

## 6. Transmutation of the singularities

As described previously, there are singular values among the permittivity distribution. However, we find that near the singular points

$$n_z \propto \begin{cases} r_{+1}^{-\frac{1}{2}} = \left[ \sqrt{(x-1)^2 + y^2} \right]^{-\frac{1}{2}}, & z \rightarrow +1, \\ r = \sqrt{x^2 + y^2}, & z \rightarrow 0, \\ r_{-1}^{-\frac{1}{2}} = \left[ \sqrt{(x+1)^2 + y^2} \right]^{-\frac{1}{2}}, & z \rightarrow -1, \end{cases} \quad (6)$$

whose singular values can then be transmuted using coordinate transformation [32]. For example, we can perform the following transformation:  $((r, \theta, z) \Leftrightarrow (R, \Theta, Z))$ ,

$$R = \begin{cases} \frac{r^2}{r_0}, & 0 \leq r \leq r_0, \\ r, & r > r_0, \end{cases} \quad \Theta = \theta, \quad Z = z \quad (7)$$

to obtain the material parameters

$$\mu_r = 2, \quad \mu_\theta = \frac{1}{2}, \quad \varepsilon_z = \frac{1}{2} \frac{b^2}{\sqrt{(x^2 - y^2 - 1)^2 + 4x^2y^2}} \quad (8)$$

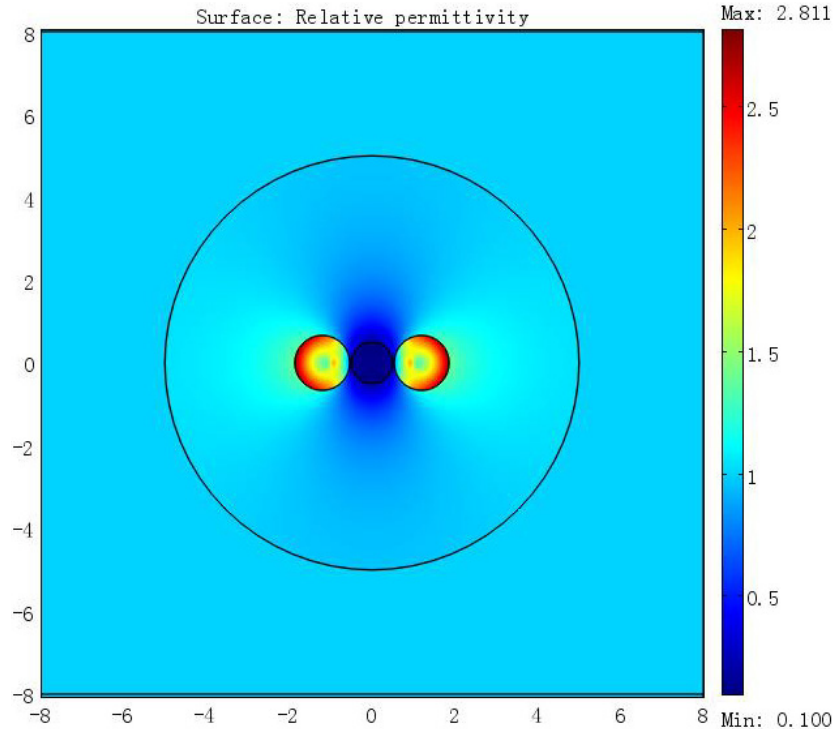


**Figure 8.** The permittivity distribution for transmuted conformal lens.

inside the region  $0 \leq r \leq r_0$ . During the simulation, we set  $r_0 = 0.5$ . For the other two singular points, it is more convenient to perform the transmutation in bipolar coordinate  $((\tau, \sigma, z) \Leftrightarrow (T, \Sigma, Z))$ ,

$$T = \begin{cases} \frac{1}{2}(\tau + \tau_0), & \tau \geq \tau_0, \\ \tau, & -\tau_0 < \tau < \tau_0, \\ \frac{1}{2}(\tau - \tau_0), & \tau \leq -\tau_0, \end{cases} \quad \Sigma = \sigma, \quad Z = z. \quad (9)$$

The transformed parameters are

$$\mu_\tau = \frac{1}{2}, \quad \mu_\sigma = 2, \quad \varepsilon_z = \frac{(\cosh \frac{1}{2}(\tau + \tau_0) - \cos \sigma)^2}{(\cosh \tau - \cos \sigma)^2} (\cosh \tau + \cos \sigma) \quad (10)$$

for  $\tau \geq \tau_0$  (or inside the region  $(x - \coth \tau_0)^2 + y^2 \leq \operatorname{csch}^2 \tau_0$ ) and

$$\mu_\tau = \frac{1}{2}, \quad \mu_\sigma = 2, \quad \varepsilon_z = \frac{(\cosh \frac{1}{2}(\tau - \tau_0) - \cos \sigma)^2}{(\cosh \tau - \cos \sigma)^2} (\cosh \tau + \cos \sigma) \quad (11)$$

for  $\tau \leq -\tau_0$  (or inside the region  $(x + \coth \tau_0)^2 + y^2 \leq \operatorname{csch}^2 \tau_0$ ). To avoid overlapping with the region  $0 \leq r \leq r_0$ , we assign  $\tau_0 = 1.2$  for instance during the simulation. Figure 8 shows the distribution of  $\varepsilon_z$ , which has no singular value now.

Figure 9(a) shows the electric field distribution when there is only one line current source (with a '1 A' current) located at the positions  $z = 0$  in the transmuted conformal lens. The far field distribution appears to be that of two line current sources (each with a '1/2 A' current) located at  $w = \pm i$  in vacuum (see also in figure 1(b)). Figure 9(b) shows the electric field

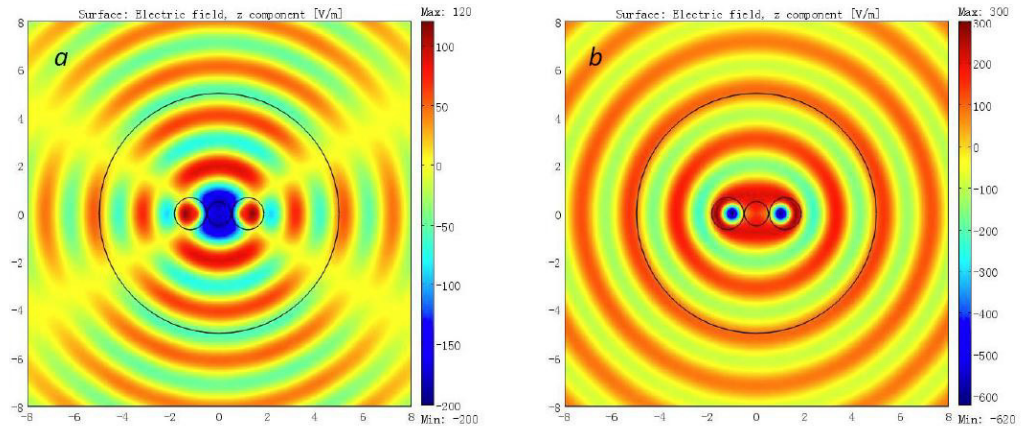


**Figure 9.** The electric field distribution for (a) one line current source with a ‘1 A’ current in the transmutated conformal lens; (b) two line current sources (each with a ‘1 A’ current) in the transmutated lens.

distribution when there are two line current sources (each with a ‘1 A’ current) located at the positions  $z = \pm 1$  in the transmutated lens. The far field distribution appears to be that of only one line current source with a ‘2 A’ current in vacuum (see also in figure 1(d)).

## 7. General mapping $w^N = z^N - 1$

Above we discuss how to transform one source into two and two into one. Now we will consider a more general conformal mapping

$$w^N = z^N - 1, \quad (12)$$

which maps  $w$ -space into  $z$ -space ( $N$  values of  $w$  are mapped into  $N$  values of  $z$ ).

The transformed refractive index in  $z$ -space is

$$n_z = \frac{|z|^{N-1}}{|z^N - 1|^{1-\frac{1}{N}}} \quad (13)$$

if the refractive index in  $w$ -space is unity. There are  $N + 1$  singular points, including  $z = 0$  (where  $n_z = 0$ ) and  $z = e^{2i\pi \frac{j}{N}}$  ( $j = 0, 1, \dots, N - 1$ ) (where  $n_z = +\infty$ ). Similar transmutation methods can be applied for finite values of the electromagnetic parameters. There are two kinds of special mappings. One is that  $z = 0$  is mapped to  $N$  points ( $w = e^{i\pi \frac{2j+1}{N}}$  ( $j = 0, 1, \dots, N - 1$ )). The other is that  $N$  singular points ( $z = e^{2i\pi \frac{j}{N}}$  ( $j = 0, 1, \dots, N - 1$ )) are mapped to  $w = 0$ . Such intriguing properties enable us to transform one active object into many and many into one. For instance, we set  $N = 3$ , while keeping the cut-off radius at  $r_c = 5$  and the wavelength  $\lambda = 2$  during the simulations. Figure 10(a) shows the electric field distribution when there is only one line current source with a ‘1 A’ current at  $z = 0$  in the conformal lens described by equation (13) (but with the cut-off radius introduced). The far field pattern appears to be that of three line current sources (each with a ‘1/3 A’ current) at the positions  $w = e^{i\frac{\pi}{3}}$ ,  $-1$ ,  $e^{i\frac{5\pi}{3}}$  in vacuum, which is plotted in figure 10(b). Figure 10(c) plots the electric field distribution for three line current sources (each with a ‘1 A’ current) located at the positions  $z = 1$ ,  $e^{i\frac{2\pi}{3}}$ ,  $e^{i\frac{4\pi}{3}}$

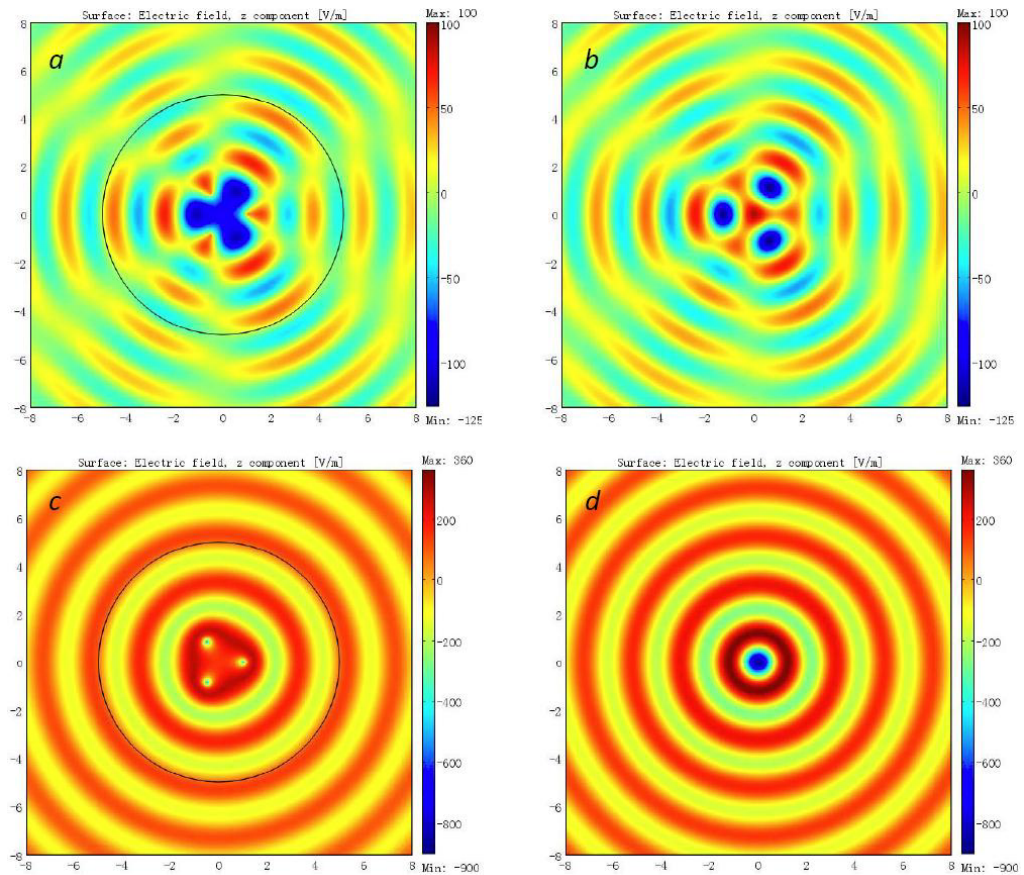


**Figure 10.** The electric field distribution for (a) one line current source with a ‘1 A’ current in the conformal lens described by equation (13) (yet with a cut-off radius); (b) three line current sources (each with a ‘1/3 A’ current) in vacuum; (c) three line current sources (each with a ‘1 A’ current) in the lens; (d) one line current source with a ‘3 A’ current in vacuum.

in the lens. It looks as if there is only one line current source with a ‘3 A’ current at  $w = 0$  in vacuum (see in figure 10(d)).

## 8. Conclusions

In conclusion, we have proposed a new class of lenses to transform one active object into many and many into one using multivalued optical conformal mapping. To the best of our knowledge, it is the first time that the effect of transforming one object into many has been discovered outside of fiction<sup>4</sup>. For the purpose of transforming multiple active objects into one, applications can be further developed in enhancing brightness for the lighting systems [34]. The conformal lenses also possess some other interesting illusion properties, such as obtaining a rotated image or changing a ‘+’ sign into a ‘-’ sign, etc. Riemann sheet analysis is used to explain the physics mechanism behind. Transmutation methods are performed to adjust the lenses for non-singular

<sup>4</sup> For example, in the famous Chinese novel, Journey to the West, by Wu Cheng En, the Monkey King can duplicate himself into many.

material parameters. Seeing the recent great progresses of the carpet cloaks [21, 23–26], as they were derived from quasi-conformal mapping [21], which more or less resembles the optical conformal mapping [35, 36], it is not difficult to foresee the future of the optical conformal devices including the conformal lenses presented herein.

## Acknowledgments

This work was supported by the National Science Foundation of China for Excellent Young Scientists (grant no. 61322504), the Foundation for the Author of National Excellent Doctoral Dissertation of China (grant no. 201217), the National Natural Science Foundation of China (grant no. 11004147), the Natural Science Foundation of Jiangsu Province (grant no. BK2010211) and the Priority Academic Program Development (PAPD) of Jiangsu Higher Education Institutions. TT acknowledges support from grant no. P201/12/G028 of the Grant Agency of the Czech Republic and from the QUEST program grant of the Engineering and Physical Sciences Research Council.

*Author contributions.* All the authors did the calculations, TT contributed the section of Riemann sheet analysis, HC conceived the idea and wrote the manuscript.

*Additional information.* Competing financial interests: The authors declare no competing financial interests.

## References

- [1] Gomez-Reino C, Perez M V and Bao C 2002 *Gradient-Index Optics: Fundamentals and Applications* (Berlin: Springer)
- [2] Maxwell J C 1854 Solutions of problems *Camb. Dublin Math. J.* **8** 188
- [3] Luneburg R K 1964 *Mathematical Theory of Optics* (Berkeley, CA: University of California Press)
- [4] Eaton J E 1952 On spherically symmetric lenses *Trans. IRE Antennas Propag.* **4** 66
- [5] Leonhardt U 2006 Optical conformal mapping *Science* **312** 1777–80
- [6] Ma Y G *et al* 2009 An omnidirectional retroreflector based on the transmutation of dielectric singularities *Nature Mater.* **8** 639–42
- [7] Kundtz N and Smith D R 2010 Extreme-angle broadband metamaterial lens *Nature Mater.* **9** 129
- [8] Smith D R *et al* 2010 Enhancing imaging systems using transformation optics *Opt. Express* **18** 21238
- [9] Smolyaninova V N *et al* 2010 Maxwell fish-eye and Eaton lenses emulated by microdroplets *Opt. Lett.* **35** 3396
- [10] Zentgraf T *et al* 2011 Plasmonic Luneburg and Eaton lenses *Nature Nanotechnol.* **6** 151
- [11] Di Falco A, Kehr S C and Leonhardt U 2011 Luneburg lens in silicon photonics *Opt. Express* **19** 5156
- [12] Danner A J, Tyc T and Leonhardt U 2011 Controlling birefringence in dielectrics *Nature Photon.* **5** 357–9
- [13] Minano J C 2006 Perfect imaging in a homogeneous three-dimensional region *Opt. Express* **14** 9627–35
- [14] Leonhardt U 2009 Perfect imaging without negative refraction *New J. Phys.* **11** 093040
- [15] Ma Y G *et al* 2011 Evidence for subwavelength imaging with positive refraction *New J. Phys.* **13** 033016
- [16] Pendry J B, Schurig D and Smith D R 2006 Controlling electromagnetic fields *Science* **312** 1780–2
- [17] Shalaev V M 2008 Transforming light *Science* **322** 384–6
- [18] Chen H Y, Chan C T and Sheng P 2010 Transformation optics and metamaterials *Nature Mater.* **9** 387–96
- [19] Schurig D *et al* 2006 Metamaterial electromagnetic cloak at microwave frequencies *Science* **314** 977–80
- [20] Cai W S, Chettiar U K, Kildishev A V and Shalaev V M 2007 Optical cloaking with metamaterials *Nature Photon.* **1** 224–7

- [21] Li J and Pendry J B 2008 Hiding under the carpet: a new strategy for cloaking *Phys. Rev. Lett.* **101** 203901
- [22] Leonhardt U and Tyc T 2009 Broadband invisibility by non-Euclidean cloaking *Science* **323** 110–2
- [23] Liu R *et al* 2009 Broadband ground-plane cloak *Science* **323** 366–9
- [24] Valentine J, Li J S, Zentgraf T, Bartal G and Zhang X 2009 An optical cloak made of dielectrics *Nature Mater.* **8** 568–71
- [25] Gabrielli L H, Cardenas J, Poitras C B and Lipson M 2009 Silicon nanostructure cloak operating at optical frequencies *Nature Photon.* **3** 461–3
- [26] Ergin T, Stenger N, Brenner P, Pendry J B and Wegener M 2010 Three-dimensional invisibility cloak at optical wavelengths *Science* **328** 337–9
- [27] Turpin J P *et al* 2009 Conformal mappings to achieve simple material parameters for transformation optics devices *Opt. Express* **18** 244–52
- [28] Ren C, Xiang Z and Cen Z 2010 Design of acoustic devices with isotropic material via conformal transformation *Appl. Phys. Lett.* **97** 044101
- [29] Yao K and Jiang X Y 2011 Designing feasible optical devices via conformal mapping *J. Opt. Soc. Am. B* **28** 1037–42
- [30] Vasic B *et al* 2010 Controlling electromagnetic fields with graded photonic crystals in metamaterial regime *Opt. Express* **18** 20321–33
- [31] Chen H Y and Chan C T 2007 Transformation media that rotate electromagnetic fields *Appl. Phys. Lett.* **90** 241105
- [32] Tyc T and Leonhardt U 2008 Transmutation of singularities in optical instruments *New J. Phys.* **10** 115038
- [33] Perczel J, Garcia-Meca C and Leonhardt U 2011 Partial transmutation of singularities in optical instruments *J. Opt.* **13** 075103
- [34] Xu Y *et al* 2011 Overlapped illusion optics: a perfect lens brings a brighter feature *New J. Phys.* **13** 023010
- [35] Leonhardt U 2009 Metamaterials: towards invisibility in the visible *Nature Mater.* **8** 537–8
- [36] Schmied R, Halimeh J C and Wegener M 2010 Conformal carpet and grating cloaks *Opt. Express* **18** 24361–67